Supplementary Information

An Electrochemically Paralleled Biomass Electrolyte Additive Facilitates the Integrated Modification of Multi-dimensional Zn Metal Batteries

Kefeng Ouyang, ‡[ab] Sheng Chen, ‡[c] Lidong Yu, ‡[d] Hongyu Qin,[ab] Ao Liu,[ab] Youfa Liu,[ab] Quan Wu,[b] Bingjie Ran,[ab] Shubing Wei,[ab] Fei Gao,[ab] Kun Zhang,[c] Jin Hu,[d] Yan Huang*[ab]

a School of Materials Science and Engineering, Harbin Institute of Technology, Shenzhen, Guangdong 518055, China.

b Sauvage Laboratory for Smart Materials, Harbin Institute of Technology, Shenzhen, Guangdong 518055, China

c Key Laboratory of Radiation Physics and Technology of Ministry of Education, Institute of Nuclear Science and Technology, Sichuan University, Sichuan 610064, China

d School of Materials Science and Engineering, Harbin Institute of Technology, Heilongjiang 150001, China

*Corresponding Author

E-mail: yanhuanglib@hit.edu.cn (Yan Huang)

Experimental Section

Preparation of electrolytes

Typically, a 2 M $ZnSO_4$ aqueous solution is employed as the base electrolyte (BE). Subsequently, aqueous solutions of PCA-Na with volume fractions of 2.5%, 5%, 10%, and 20% are prepared and used as solvents for the preparation of 2 M $ZnSO_4$ electrolytes containing varying concentrations of additives. For the assembly of Zn||MnO_2 cells, an additional 0.2 M $MnSO_4$ is incorporated into the electrolyte. Regarding the alkaline electrolyte, deionized water and 10% PCA-Na aqueous solution are utilized as solvents to prepare pure and modified 6 M KOH + 0.2 M zinc acetate electrolyte.

Preparation of α-MnO_2 and I_2@AC cathode materials

To synthesize α-MnO_2, 6 mmol $MnSO_4 \cdot H_2O$ and 4 mL 0.5 mol L^{-1} H_2SO_4 were dissolved in 120 mL deionized water under magnetic stirring for 10 min, and then, 40 mL 0.1 mol L^{-1} $KMnO_4$ was slowly dropped into the above solution. The mixture was stirred for 1 h, followed by sonication for 1 h. Finally, the mixture was transferred into a Teflon-lined autoclave and heated at 120°C for 12 h. After cooling to room temperature, α-MnO_2 was washed with distilled water and dried overnight at 60°C in a vacuum drying oven. I_2@AC was synthesized through a facile method. Briefly, iodine was mixed with activated carbon in a 1:1 mass ratio and sealed within a 100 mL hydrothermal PTFE reactor, which was then heated at 90°C for 12 h. After natural cooling, I_2@AC was obtained.

Assembly of Zn||Zn symmetric and Zn||Cu asymmetric coin/pouch cells

In this work, unless otherwise noted, Zn discs with a thickness of 100 μm were typically employed as Zn anodes. CR2032-type Zn||Zn symmetric coin cells were assembled using Zn anodes with a diameter of 12 mm and GF/D glass fiber separators. For Zn||Zn pouch symmetric cells, the dimensions of the Zn anodes were 10 cm × 10 cm. During DOD testing, Zn anodes with a thickness of 50 μm were employed. As for asymmetric Zn||Cu coin/pouch cells, copper foils with a thickness of 10 μm, equivalent in area to the Zn anodes, are utilized as the copper cathodes.

Assembly of alkaline Zn-air cells

Pt/C catalyst (20% Pt) and an appropriate amount of Nafion binder were dissolved in Vol 20% ethanol solution to prepare the catalyst ink. This ink was then applied onto carbon paper and dried naturally to fabricate the oxygen catalytic electrode. A 500 μm thick Zn anode was coupled with catalytic electrode and assembled into a 30 mL capacity fuel cell casing mold, which was subsequently filled with the alkaline electrolyte.

Assembly of Zn||α-MnO_2 coin/pouch cells

To assemble aqueous Zn||MnO_2 coin cells, the cathode was prepared by dissolving α-MnO_2 powder, Ketjen black EC-300J, and PVDF 900 in NMP at a weight ratio of 7:2:1, followed by thorough mixing. The resulting slurry was coated onto carbon cloth and dried overnight under vacuum at 60°C. The MnO_2 mass loading of the obtained cathode was controlled at 1 mg cm^{-2}. Zn anodes were coupled with the prepared MnO_2 cathode, and Mn^{2+}-containing electrolytes were employed to assemble the coin cells. For the pouch cells, the cathode was fabricated by mixing and dissolving α-MnO_2 powder, Ketjen black EC-300J, and CMC 200 in deionized water at a weight ratio of 7:2:1. The slurry was then coated onto a 10 cm × 10 cm stainless steel mesh, followed by repeated drying and rolling to obtain the final electrode (MnO_2 loading $\approx$ 30 mg cm^{-2}). One obtained electrode was then coupled with two 10 cm × 10 cm Zn anodes to assemble Zn||MnO_2 pouch cells.

Assembly of Zn||I_2 coin/pouch cells

All I_2 cathodes were fabricated using a consistent method. Specifically, the prepared I_2@AC cathode material was mixed with Ketjen black and CMC in a mass ratio of 8:1:1, followed by dissolution in deionized water to form a viscous slurry. This slurry was then coated onto both sides of a 10 cm × 10 cm titanium mesh (Note: for coin cell electrodes, only one side requires coating, and the electrode should be trimmed prior to assembly). After multiple drying and roller pressing steps, a dense I_2 cathode was obtained. During coin cell assembly, one Zn anode was coupled with one I_2 cathode. For the assembly of pouch cells, four anodes and three I_2 cathodes were alternately stacked, with a GF/D separator placed between each anode and cathode.

Material Characterizations

X-ray diffraction (XRD) analysis was conducted using a PANalytical Empyrean with CuKα radiation (λ=1.54065 Å). Fourier transform infrared (FTIR) spectra were recorded using an IR Affinity-1s. Scanning electron microscopy (SEM) combined with energy dispersive X-ray spectroscopy (EDS) was performed using a JEOL JSM-7800F equipped with an Ametek TEAM Octane Plus. Operando optical observations were conducted using a Motic BA310Met paired with a CHI760e electrochemical workstation (Shanghai Chenhua). Atomic force microscopy (AFM) images, obtained using a Dimension Icon system, were used to assess the surface smoothness of cycled Zn anodes. The in situ pH monitoring was performed with a PHSJ-6L (Shanghai Leici) connected to a CHI760e electrochemical workstation (Shanghai Chenhua).

Electrochemical measurements

The galvanostatic charge/discharge of cells at different working conditions were carried out on CT3001A cell testing system (Wuhan LAND Electronic Co. Ltd.) or CT-4008Tn cell testing system (Shenzhen, NEWARE). The tests of CA, Tafel, HER, and CV curves were obtained by a 1470E electrochemical workstation (Solartron Analytical, Ametek) or CHI760e electrochemical workstation (Shanghai Chenhua).

The formula used to calculate the DOD for a Zn metal anode using Zn foil is as follows:

$$\mathrm{DOD}=\frac{y}{C_{Zn,\,volume}\cdot x}\times 10^{-4}\times 100\% = \frac{y}{0.585x}\times 100\%$$

where x (μm) is the thickness of the Zn foil, y (mAh cm^{-2}) represents the Zn areal capacity used in electrochemical testing and $C_{\mathrm{Zn,volume}}$ is the volume capacity (5855 mAh cm^{-3}).

DFT calculation

Density functional theory (DFT) calculations between molecules and ions were performed using the Gaussian 16 program.[1] The additives and H_2O molecules were geometrically optimized at a level of PBE0-D3 (BJ)/def2-SVP. The energies of H_2O and PCA^- with other molecules were calculated at a level of M06-2X/def2-TZVP. All binding energy calculations have undergone basis set superposition error (BSSE) correction. The binding energy (E_b) is calculated according to the following equation:

$$E_b=E_{total}-E_A-E_B+E_{BSSE}$$

E_A, E_B, and E_{total} are the energies of the separated molecules (A or B), as well as the total energy of the complex structures of A and B. E_{BSSE} is the energy that eliminates the influence of BSSE through counterpoise. The molecular orbitals and electrostatic potential on the molecular surface were obtained through Multiwfn[2,3] and VMD[4] programs.

Adsorption energy calculations were performed using spin-polarized and periodic DFT implemented in the Vienna Ab initio Simulation Package (VASP) code.[5] The exchange-correlation potential was treated by using a generalized gradient approximation (GGA) using the Perdew-Burke-Ernzerhof (PBE) parametrization.[6] Additionally, the van der Waals correction of Grimme's DFT-D3 model was also adopted.[7] After geometry optimization, the lattice constants are determined as follows : $a = b = 13.06$ Å and $\gamma = 120°$. Meanwhile, a vacuum region of about 15 Å was applied to avoid the interaction between adjacent images. The energy cutoff was set to be 450 eV. The Brillouin-zone integration was sampled with a Γ-centered Monkhorst-

Pack mesh[8] of 2 × 2 × 1. The structures were fully relaxed until the maximum force on each atom was less than 0.02 eV/Å, and the energy convergent standard was 10^{-5} eV. The Adsorption energy (ΔE) is defined as, $\Delta E = E_{*ads} - E_{*} - E_{ads}$, where E_{*ads} is the energy adsorbed by the adsorbent on the surface, E_{*} is the energy of the surface, and E_{ads} is the energy of the adsorbent under vacuum.

Molecular dynamics (MD) simulations

The MD simulations were carried out using GROMACS 2024. The SPC/E model is used to describe water. For the other molecules and ions, Amber and GAFF force fields are employed to describe the non-bonded interaction. The molecules were optimized at the B3LYP/def2svp level by Gaussian 16, and then calculated at single points in gas and water (IEFPCM) at the B3LYP/def2tzvp level by Gaussian 16, respectively. The simulation system with Salicin additives contains 3764 H_2O, 150 Zn^{2+}, 150 SO_4^{2-} and 60 PCA^-,60 Na^+, and the pure $ZnSO_4$ system includes 4182 H_2O, 150 $Zn^{2+}$and 150 SO_4^{2-}. Particle-Mesh-Ewald (PME) methods were utilized to compute the electrostatic interactions. A cutoff length of 1.2 nm was used in the calculation of electrostatic interactions and non-electrostatic interactions in real space and the integration time step was 1 fs. After that, a molecular dynamic of 5 ns at constant temperature (298.15 K) and pressure (1 bar) (NPT) was performed for this system, which brought them into a reasonable pre-equilibrated configuration for subsequent simulations. Finally, a 10-ns production simulation was conducted for post-processing analysis. The charges of ions were scaled by 0.8 to overcome the too strong interaction between cations and anions.

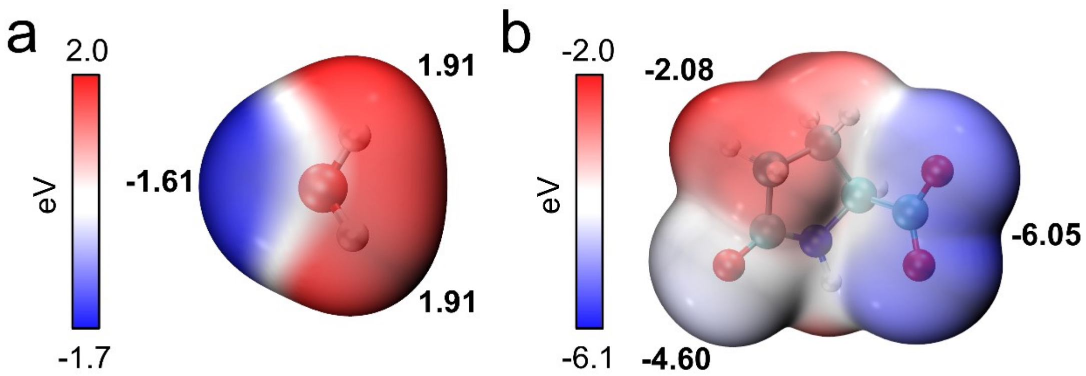

Figure S1. Electrostatic potential on the van der Waals surface of (a) H_2O and (b) PCA^-.

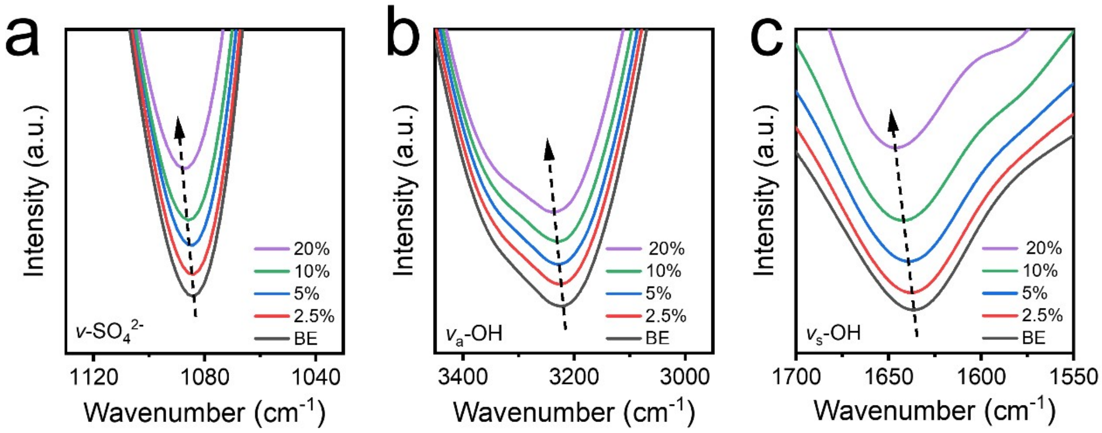

Figure S2. The FTIR spectra of characteristic peaks of (a) v-SO_4^{2-}, (b) v_a-OH and (c) v_s-OH in different electrolytes.

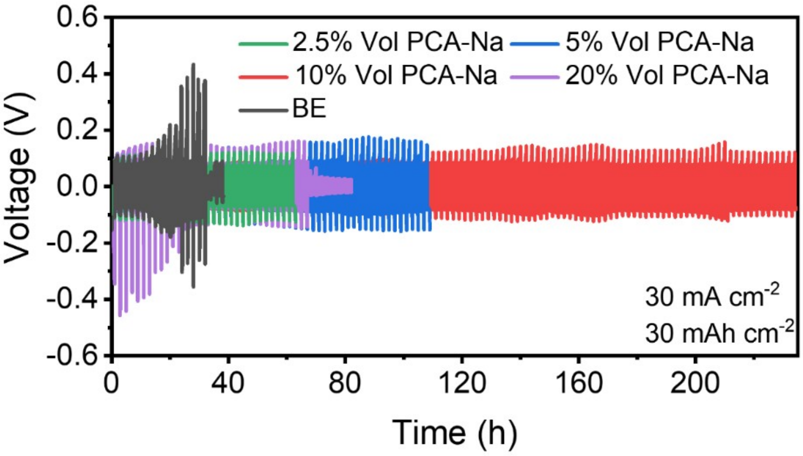

Figure S3. Cycling performance of Zn||Zn symmetric cells using different electrolytes at 30 mA cm^{-2}, 30 mAh cm^{-2}.

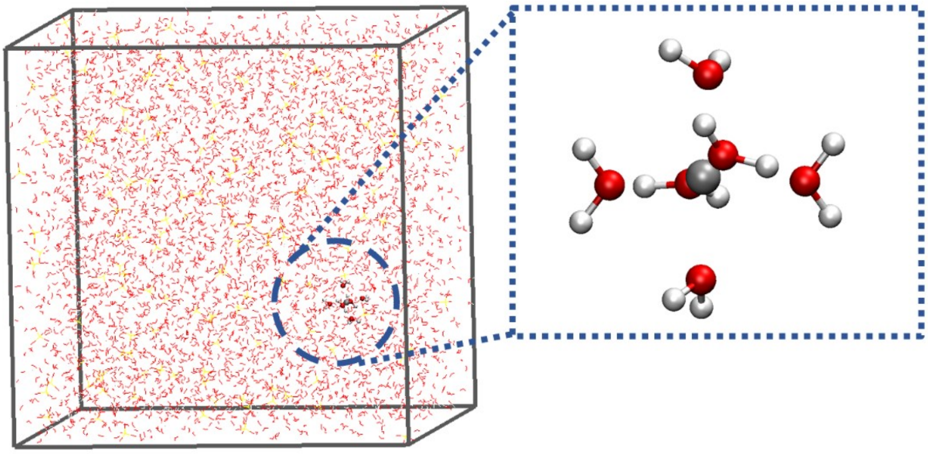

Figure S4. Snapshot of the MD simulation cells for BE.

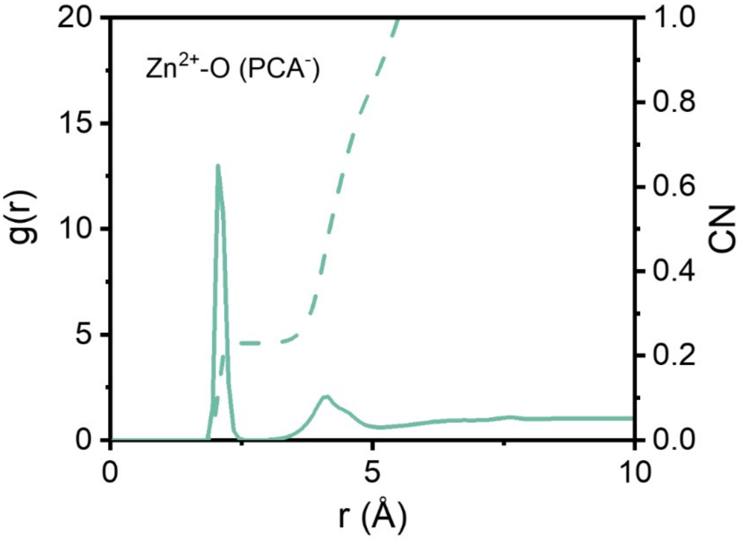

Figure S5. The radial distribution functions of Zn^{2+}-O (PCA^-) and the radius-dependent coordination numbers in EPBE.

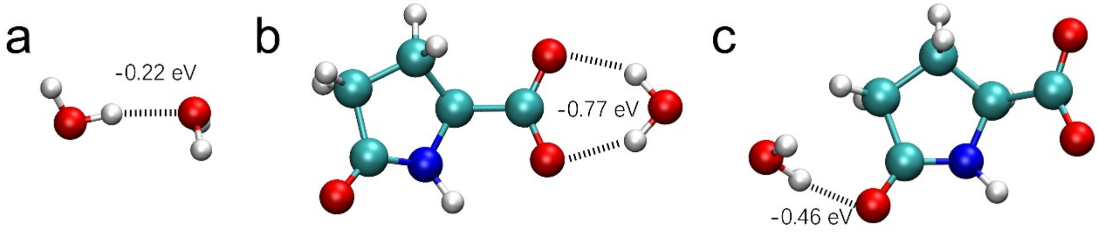

Figure S6. Binding energies between (a) water molecules, (b) water molecule and the carbonyl group of PCA$^-$, and (c) water molecule and the carboxyl group of PCA$^-$.

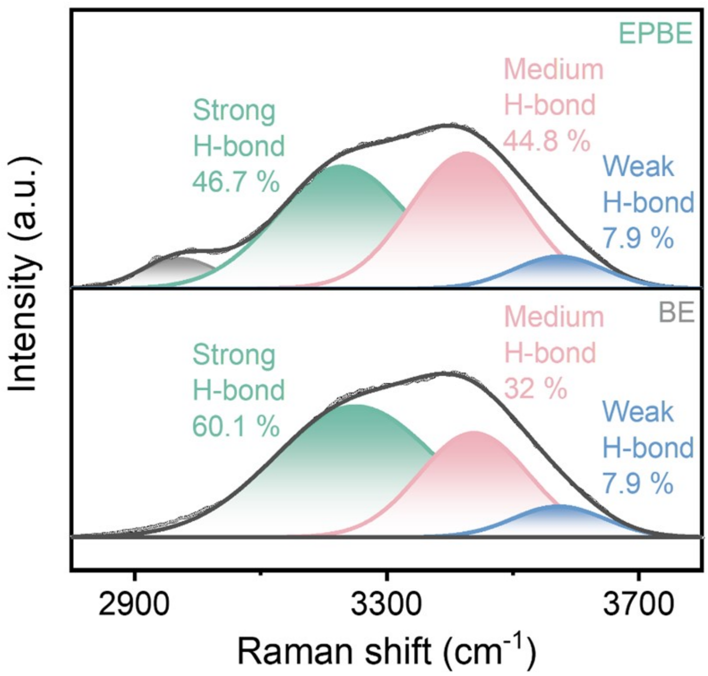

Figure S7. The fitted Raman characteristic peaks of water molecules in BE and EPBE.

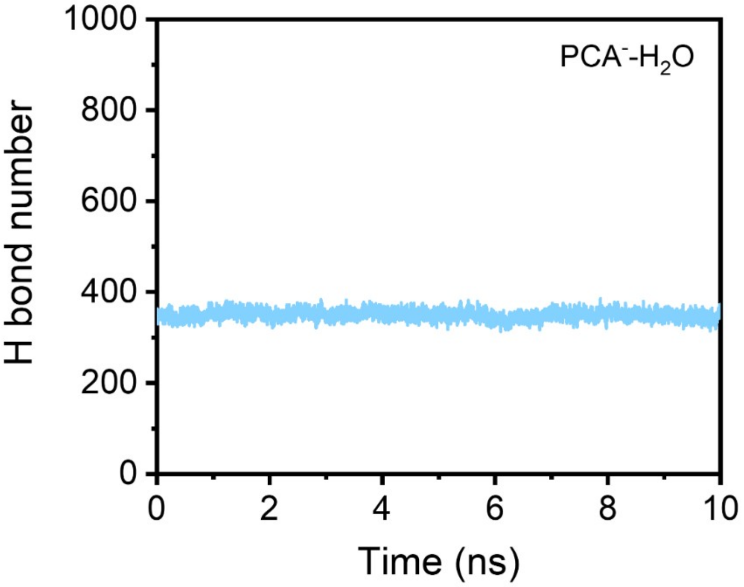

Figure S8. The number of hydrogen bonds between PCA$^-$ and water molecules in EPBE derived from MD simulations.

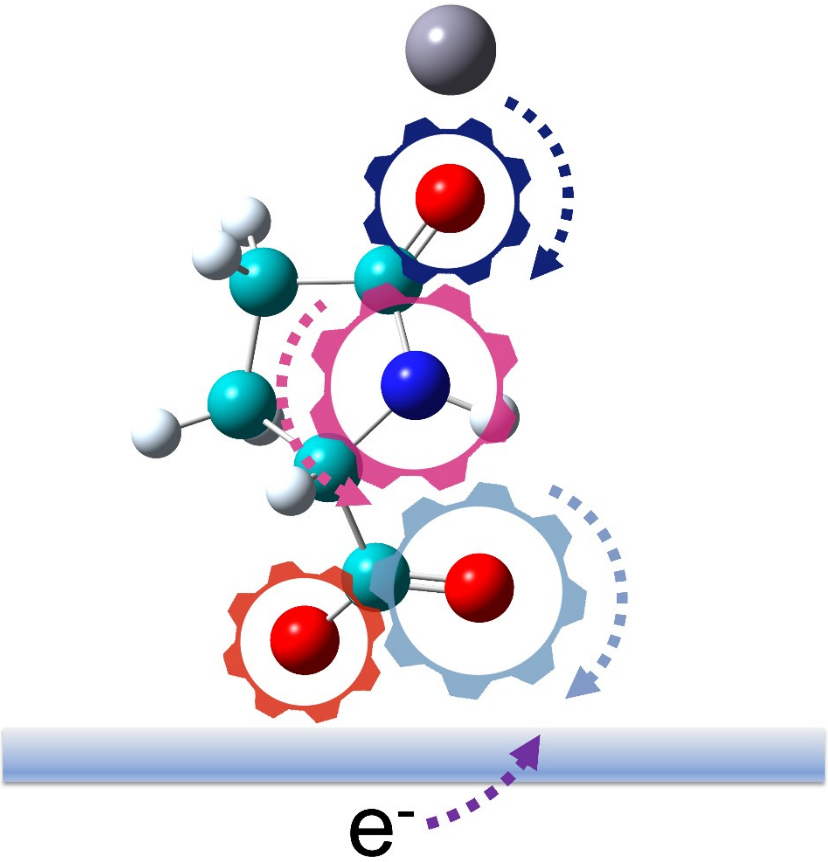

Figure S9. Schematic diagram of Zn^{2+} interfacial transport pathway on the surface of Zn anode regulated by PCA^-.

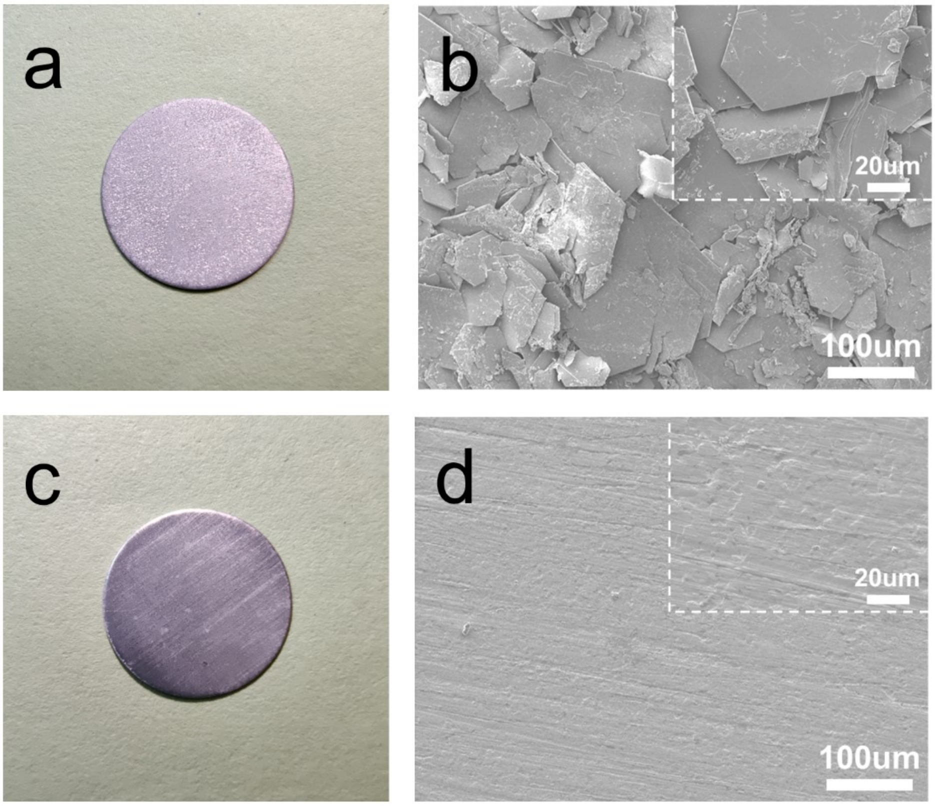

Figure S10. The digital photographs and corresponding SEM images of Zn anodes soaked for seven days in (a, b) BE and (c, d) EPBE.

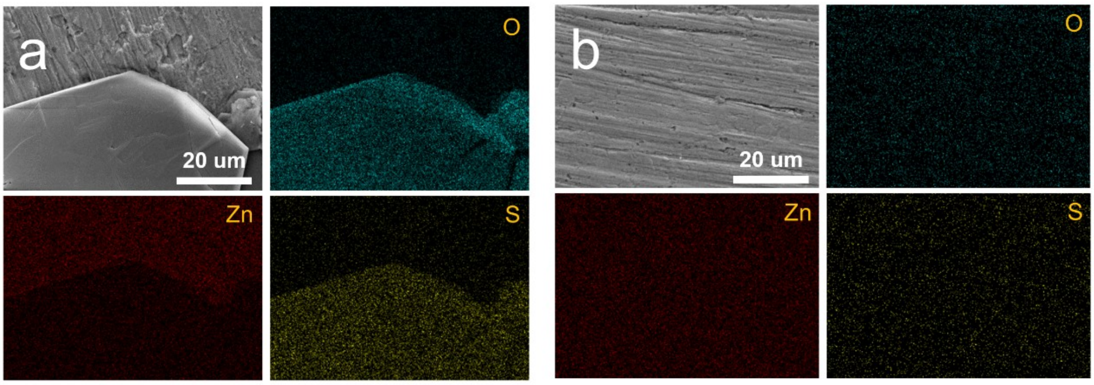

Figure S11. EDS spectra of Zn anodes immersed in (a) BE and (b) EPBE for seven days.

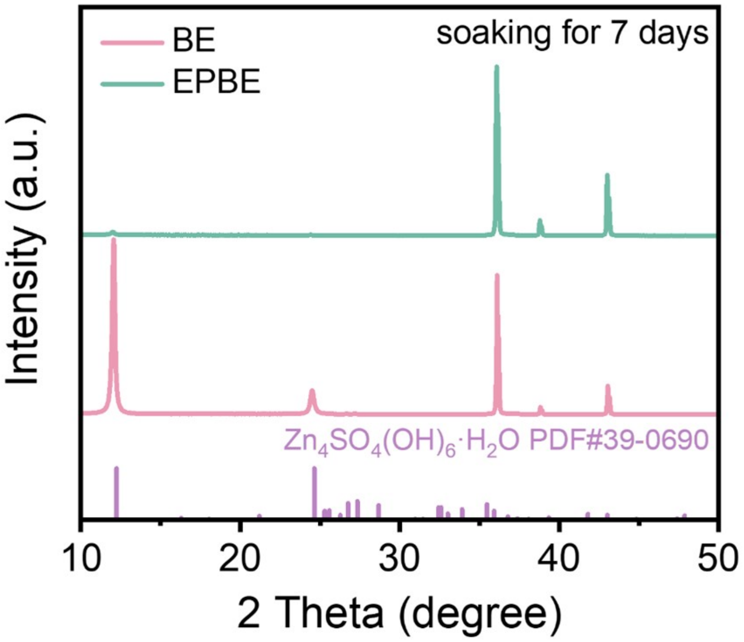

Figure S12. XRD patterns of Zn anodes immersed in BE and EPBE for seven days.

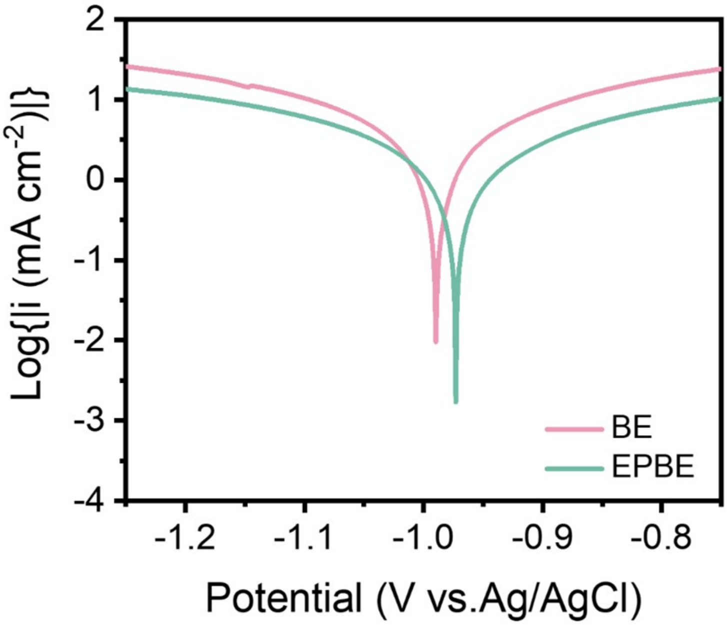

Figure S13. Tafel curves of the Zn anode in BE and EPBE.

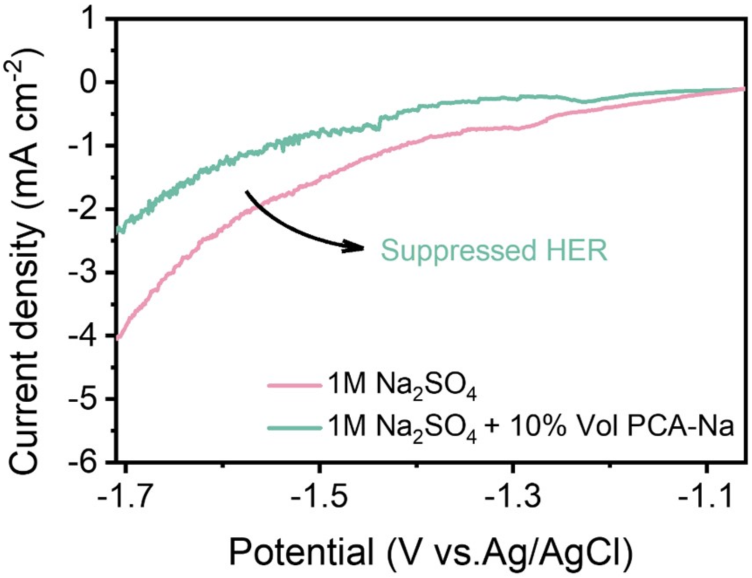

Figure S14. HER curves of the Zn anode in 1 M Na_2SO_4 and 1 M Na_2SO_4 + 10% Vol PCA-Na.

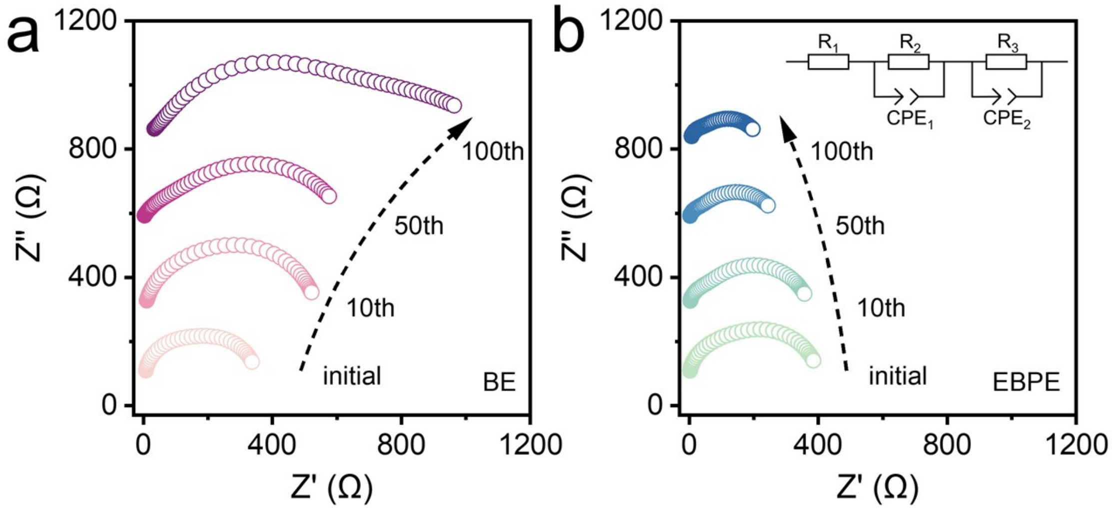

Figure S15. Nyquist plots of the Zn||Zn symmetric cells using the (a) BE and (b) EPBE after different cycles at 5 mA cm^{-2}, the illustration depicts the equivalent circuit schematic.

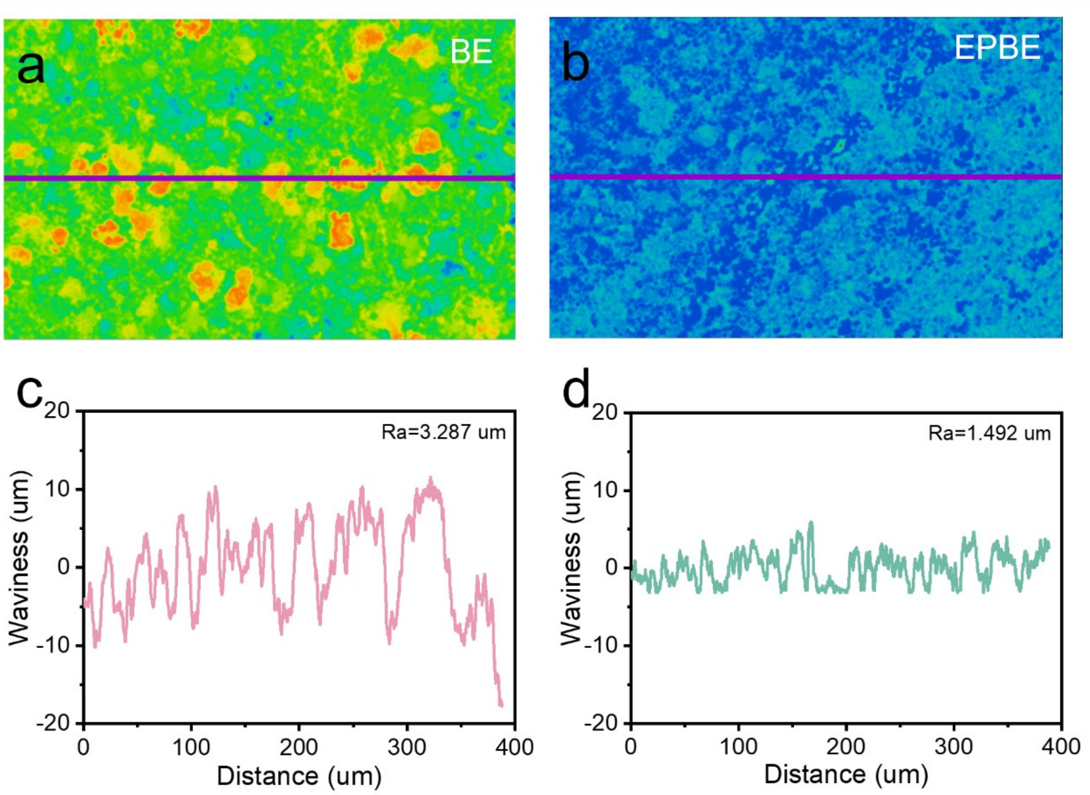

Figure S16. Corresponding 2D profilometer images and waviness (corresponding to the line-marked position in the 2D images) of anodes after cycling for 50 times at 5 mA cm^{-2} and 5 mAh cm^{-2} in (a, c) BE and (b, d) EPBE.

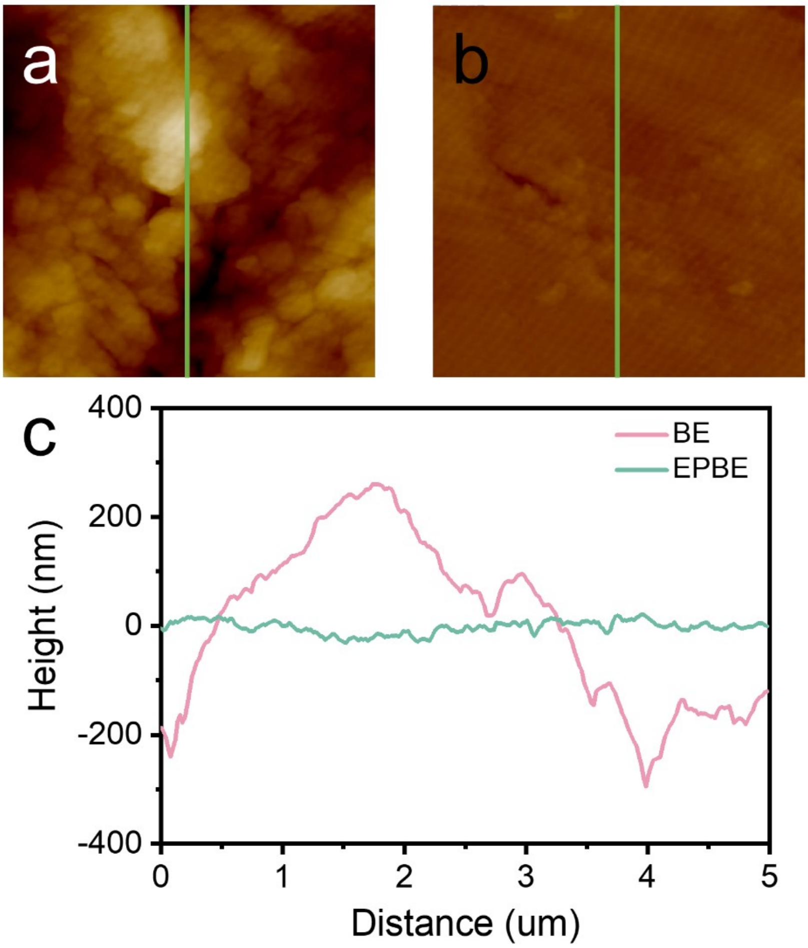

Figure S17. Corresponding 2D AFM images of anodes after cycling for 50 times at 5 mA cm^{-2} and 5 mAh cm^{-2} in (a) BE and (b) EPBE, and the comparison of surface roughness (corresponding to the line-marked position in the 2D images).

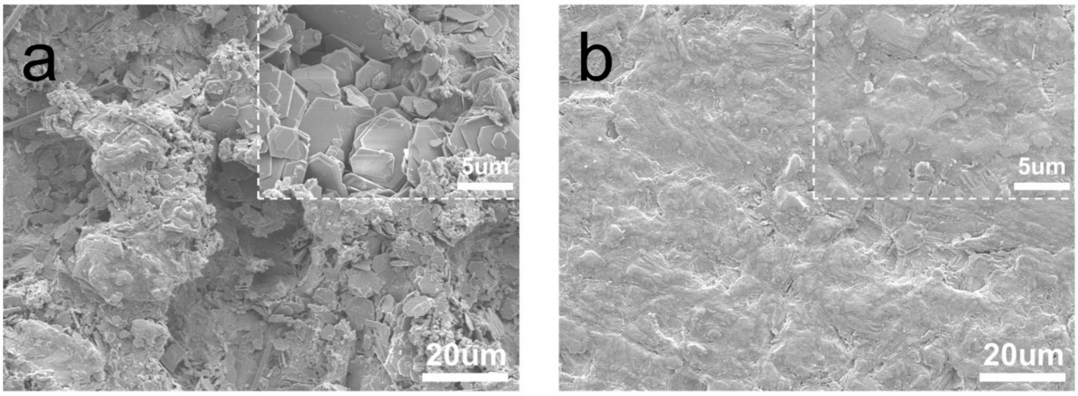

Figure S18. SEM images of anodes before and after cycling for 50 times at 5 mA cm^{-2} and 5 mAh cm^{-2} in (a) BE and (b) EPBE.

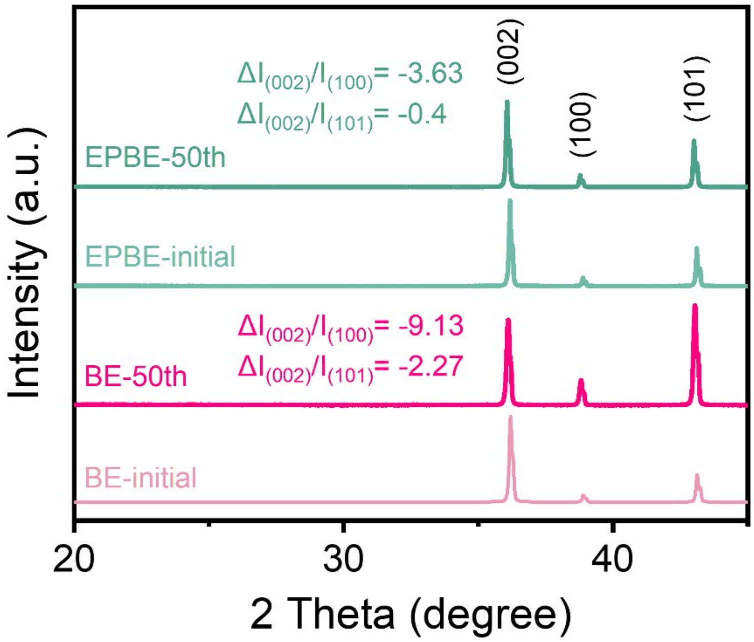

Figure S19. XRD patterns of anodes before and after cycling for 50 times at 5 mA cm^{-2} and 5 mAh cm^{-2} in BE and EPBE.

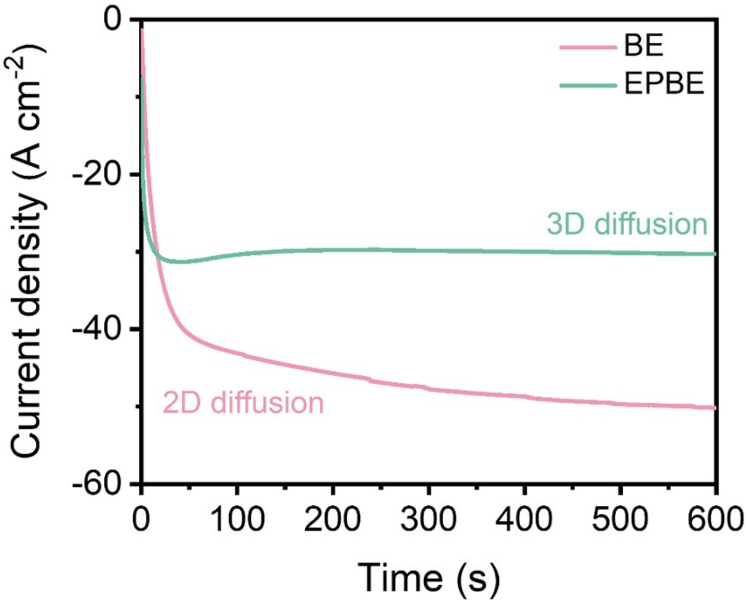

Figure S20. CA curves of Zn anodes in BE and EPBE at a fixed overpotential of -150 mV.

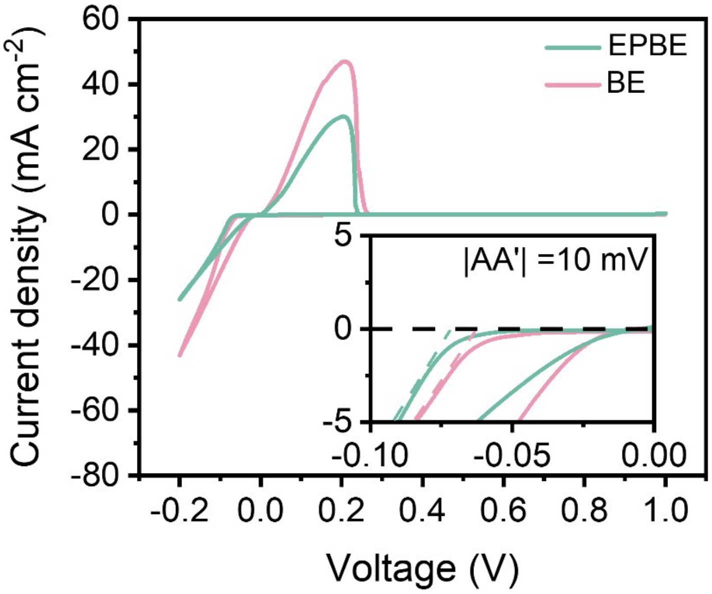

Figure S21. CV curves recorded at 0.2 mV s^{-1}, insert compared the nucleation overpotential of Zn^{2+} in BE and EPBE.

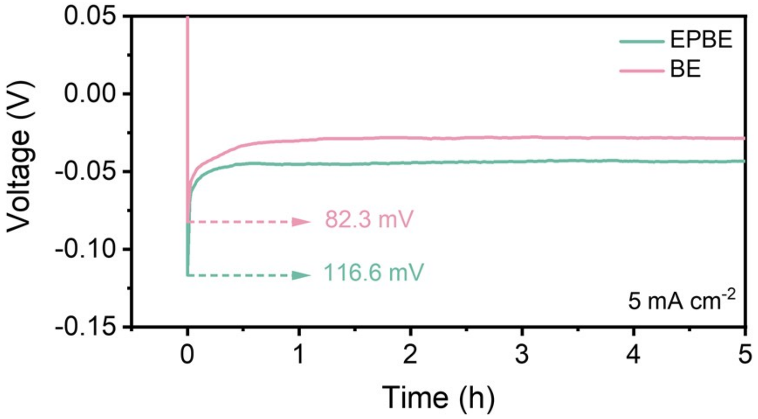

Figure S22. The overpotential of Zn||Cu asymmetric cells using BE and EPBE.

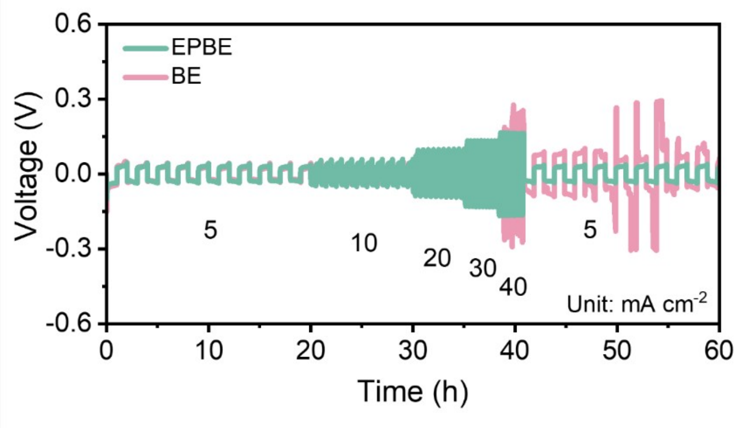

Figure S23. Rate performance comparison of Zn anodes in BE and EPBE.

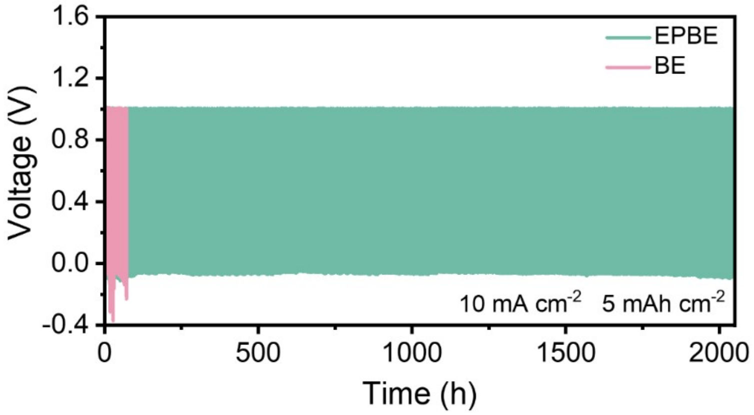

Figure S24. Comparison of cycling performance of Zn||Cu asymmetric cells using BE and EPBE.

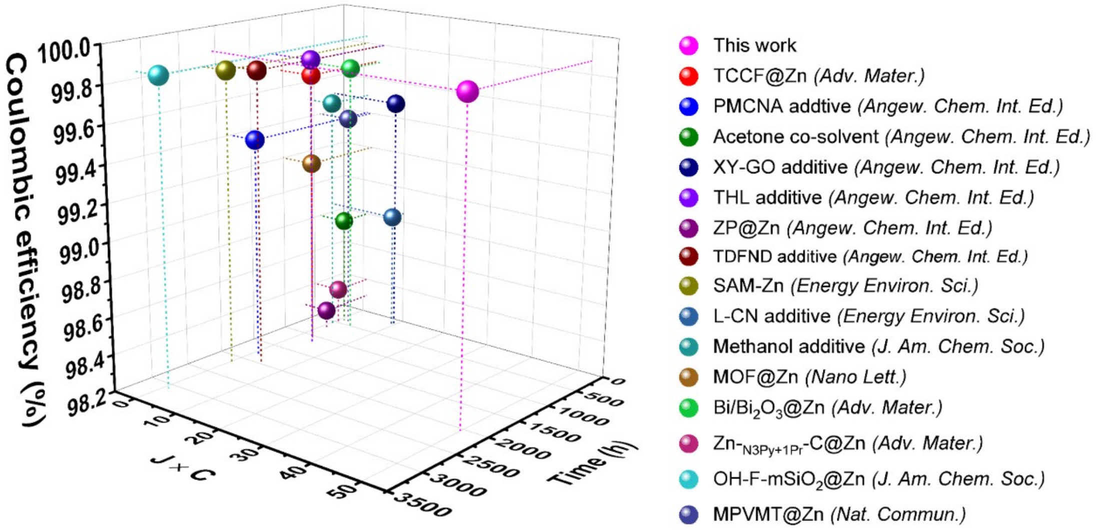

Figure S25. Comparison of coulombic efficiency between this work and other previous reports (J = current density/mA cm^{-2}, C = areal capacity/mAh cm^{-2}).

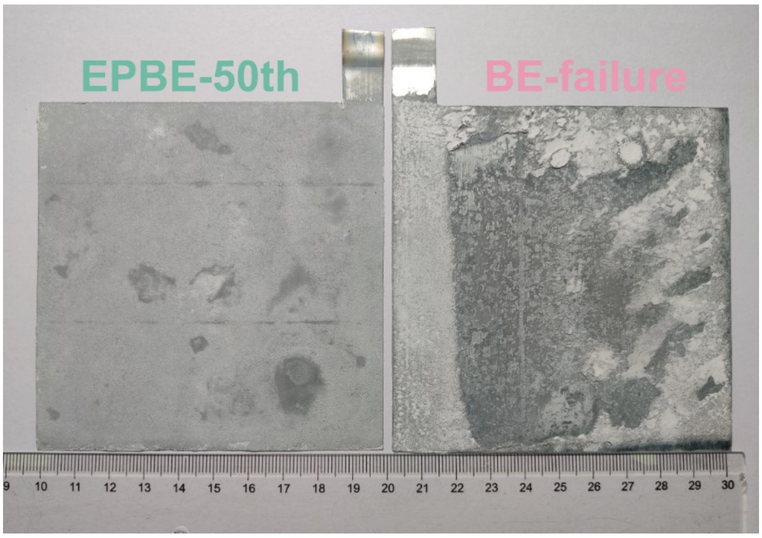

Figure S26. Zn anodes of Zn||Zn pouch cells cycled for 50 cycles at 10 mA cm^{-2} and 10 mA cm^{-2} in BE and EPBE.

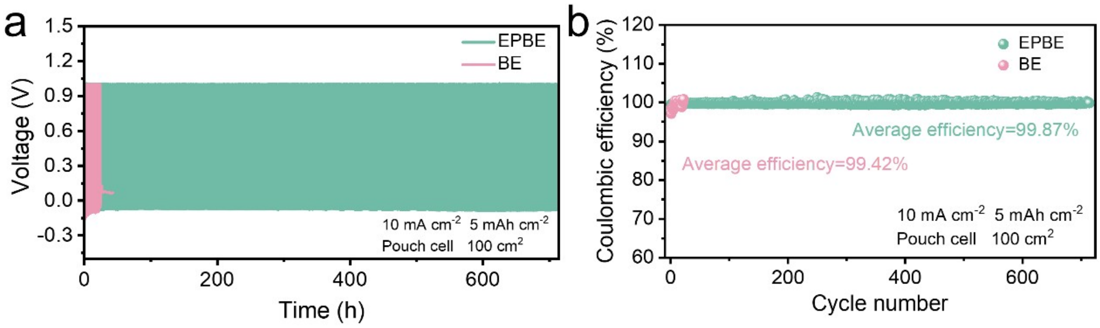

Figure S27. Comparison of (a) cycling performance and (b) corresponding coulombic efficiency of Zn||Cu asymmetric pouch cells using BE and EPBE.

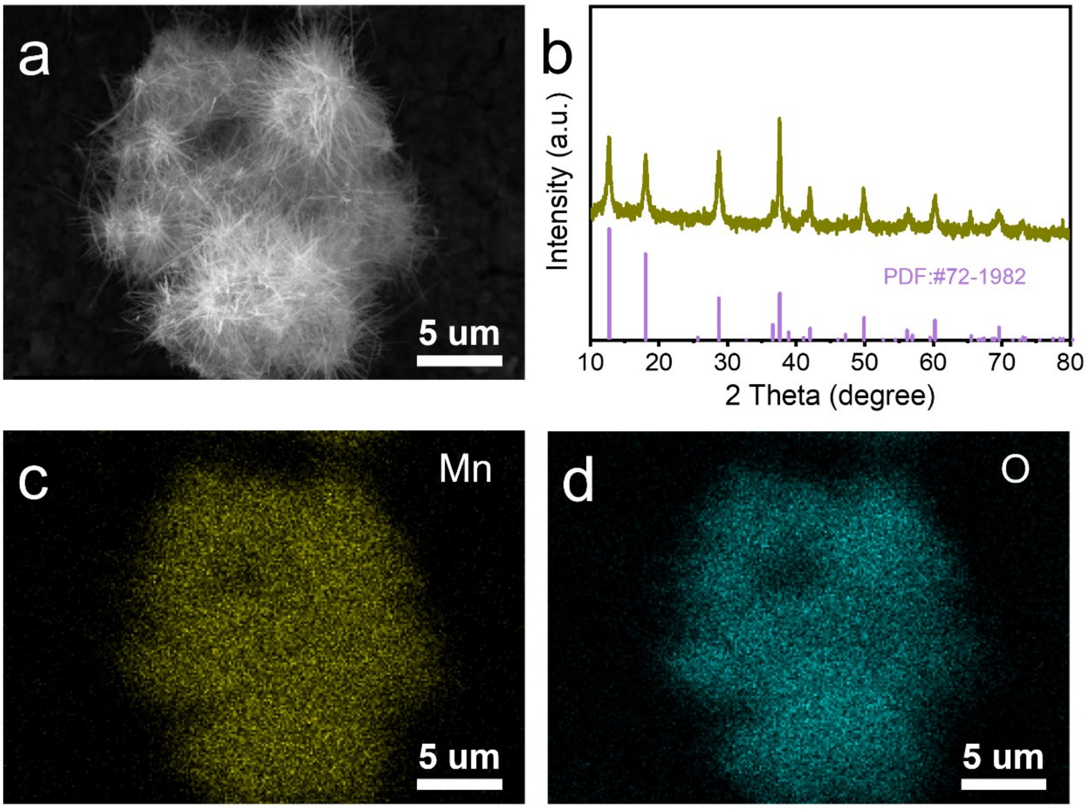

Figure S28. (a) SEM image, (b) XRD and (c, d) EDS images of α-MnO_2.

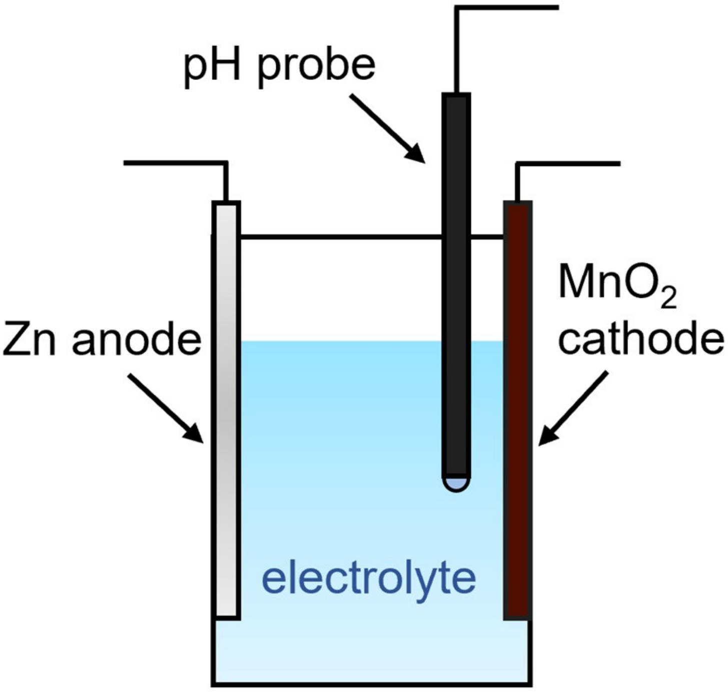

Figure S29. Schematic diagram of the in situ pH testing.

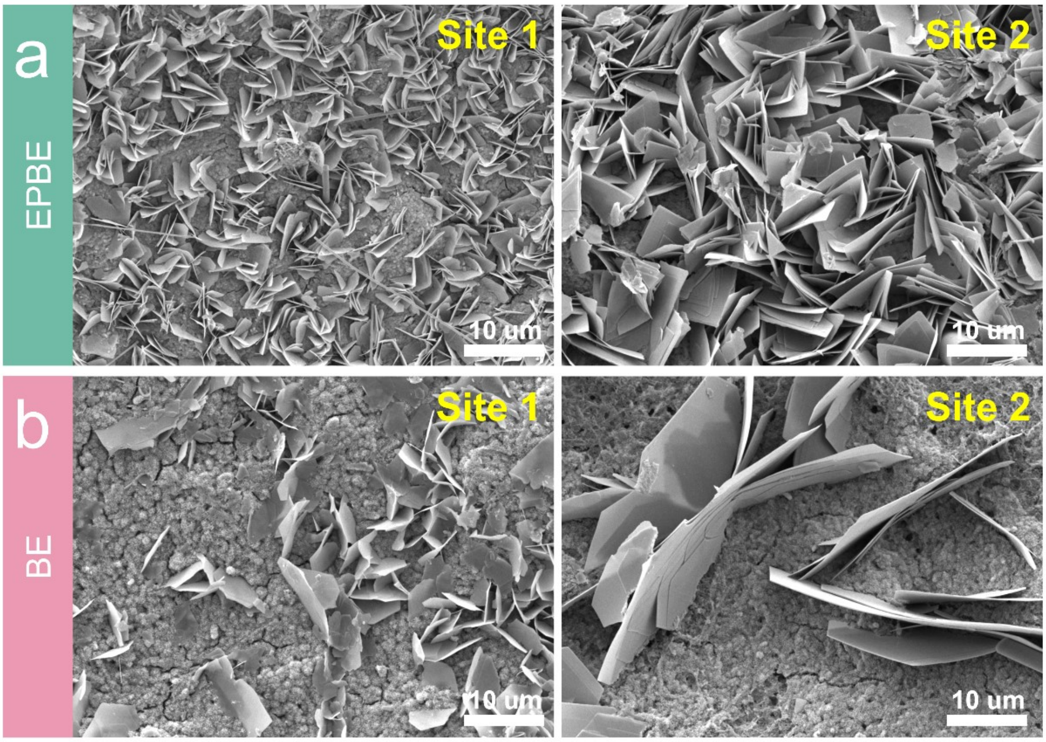

Figure S30. SEM images of the surface of the MnO_2 cathode operating in BE and EPBE, corresponding to site 1 and site 2 on the time-voltage curve.

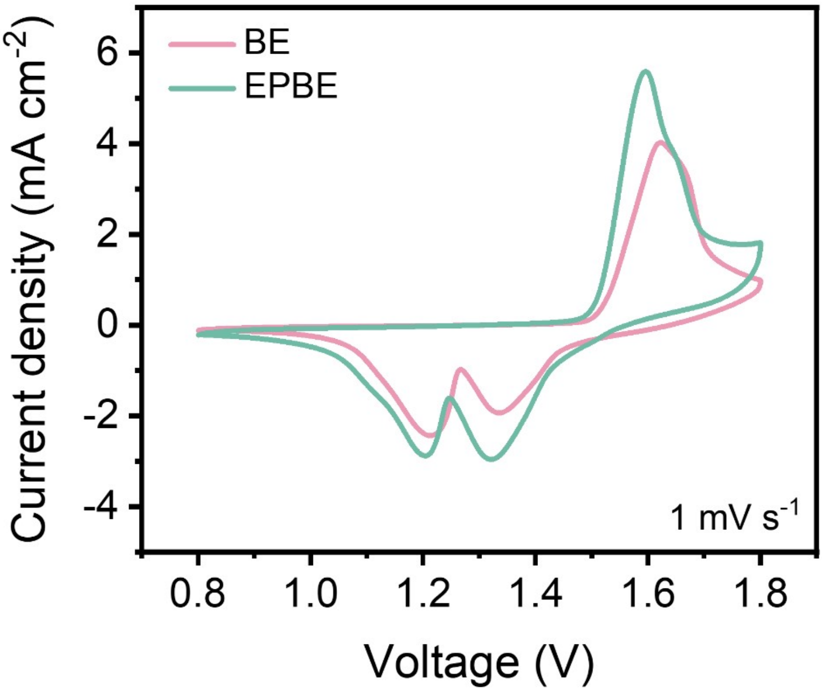

Figure S31. The comparison of CV curves of Zn||MnO$_2$ using BE and EPBE at a sweep speed of 1 mVs $^{-1}$**.**

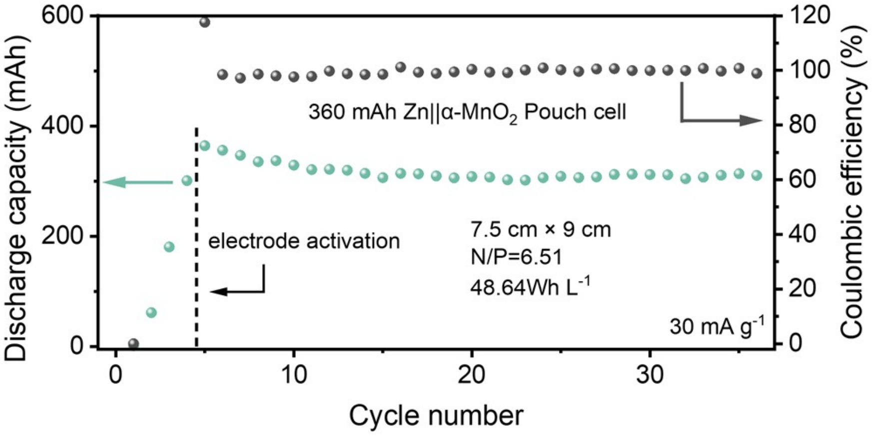

Figure S32. Long-term cycling performance of Zn||MnO$_2$ pouch cells with a cathode size of 7.5 cm × 9 cm and a Zn anode thickness of 30 µm.

Figure S33. Digital images of ABE and AEPBE in the initial state.

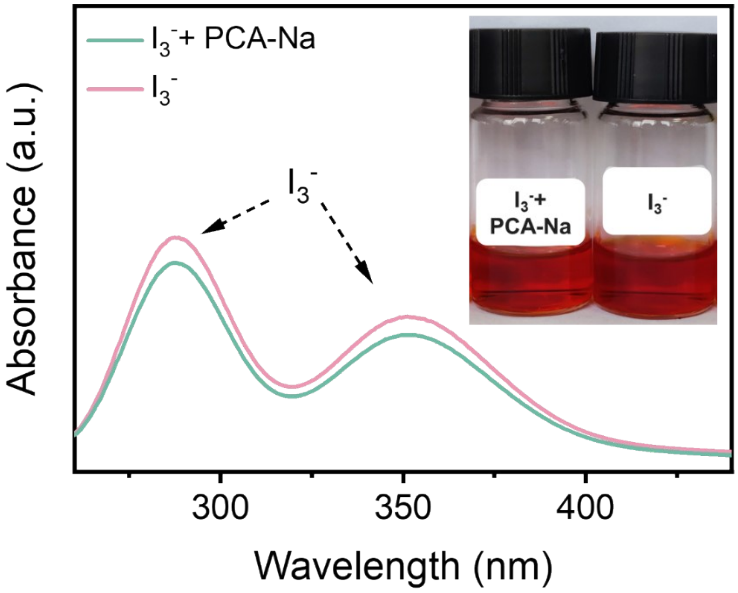

Figure S34. UV–vis spectrum of I_3^- in I_3^- solution and I_3^-+PCA-Na solution at the initial state, and the corresponding digital images.

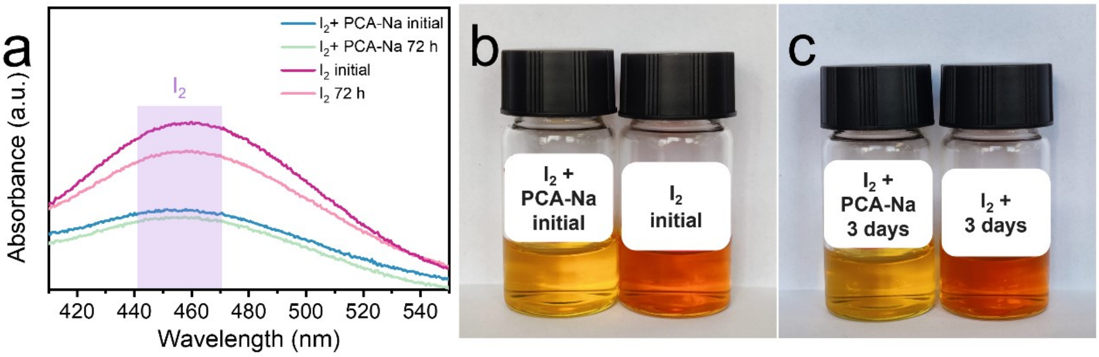

Figure S35. (a) UV–vis spectrum of I_2 in I_2 solution and I_2 + PCA-Na solution at the initial state and after 72 h of standing, (b) and the corresponding digital images.

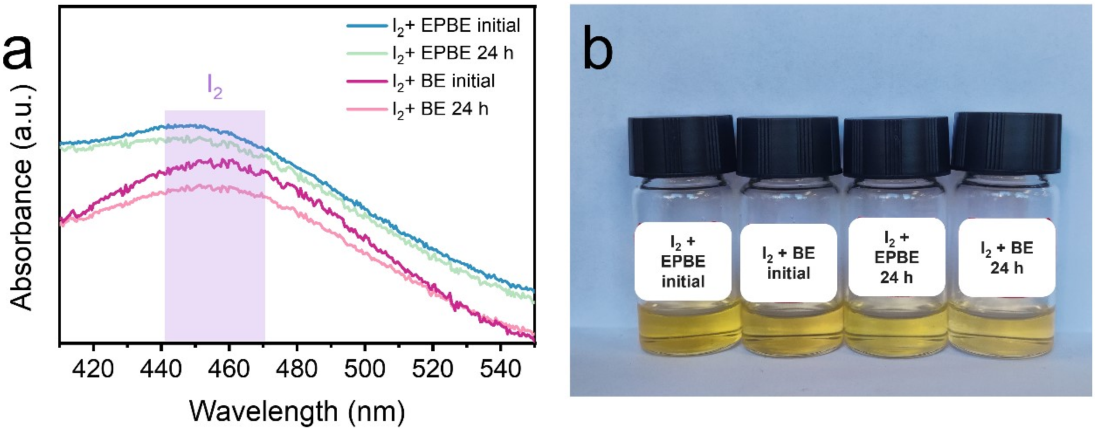

Figure S36. (a) UV–vis spectrum of I_2 in I_2 + EPBE and I_2 + BE at the initial state and after 24 h of standing, (b) and the corresponding digital images.

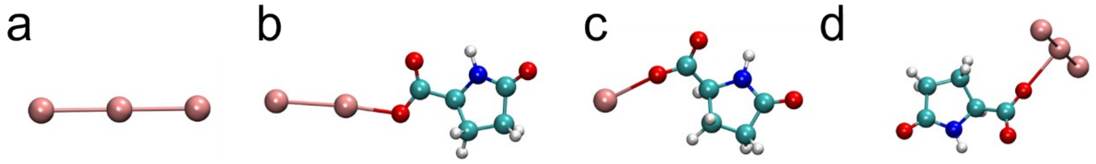

Figure S37. The molecular models constructed for calculating the interaction between (a) I^- and I_2, (b) I_2 and PCA^-, (c) I^- and PCA^-, (d) I_3^- and PCA^-.

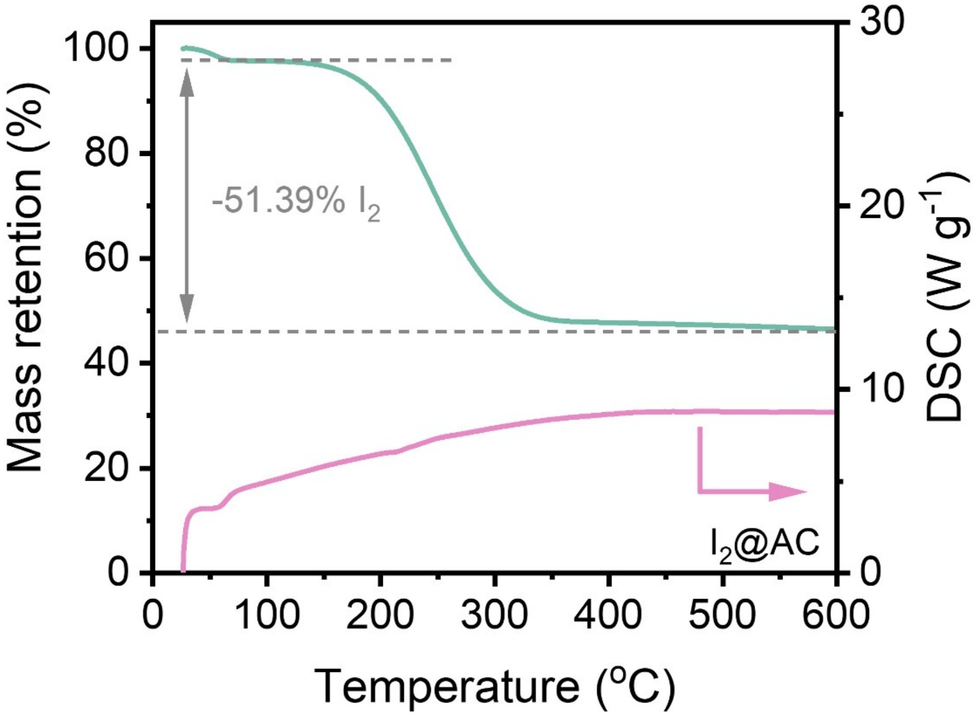

Figure S38. TG analysis of the synthesized I_2@AC.

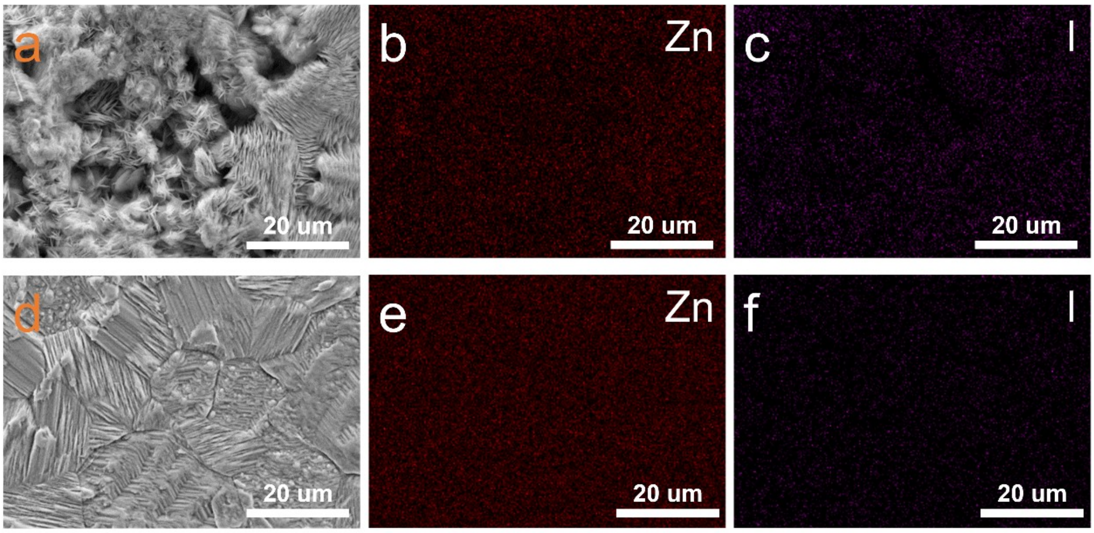

Figure S39. SEM and EDS images of the Zn anode of the Zn||I_2 cell using (a-c) BE and (d-f) EPBE after 50 cycles.

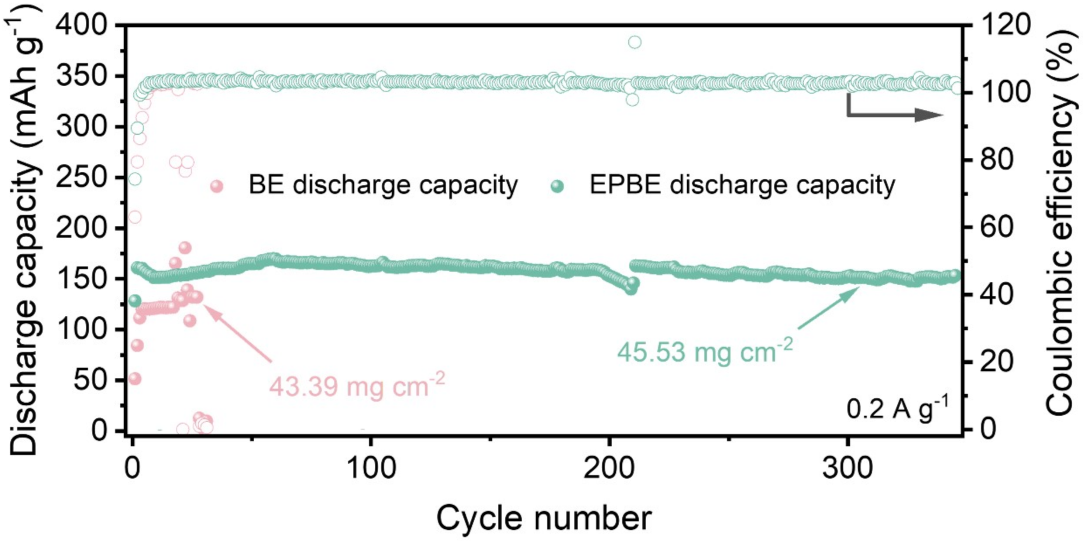

Figure S40. Cycle performance of the Zn||I_2 cells with high iodine loading at 0.2 A g^{-1}.

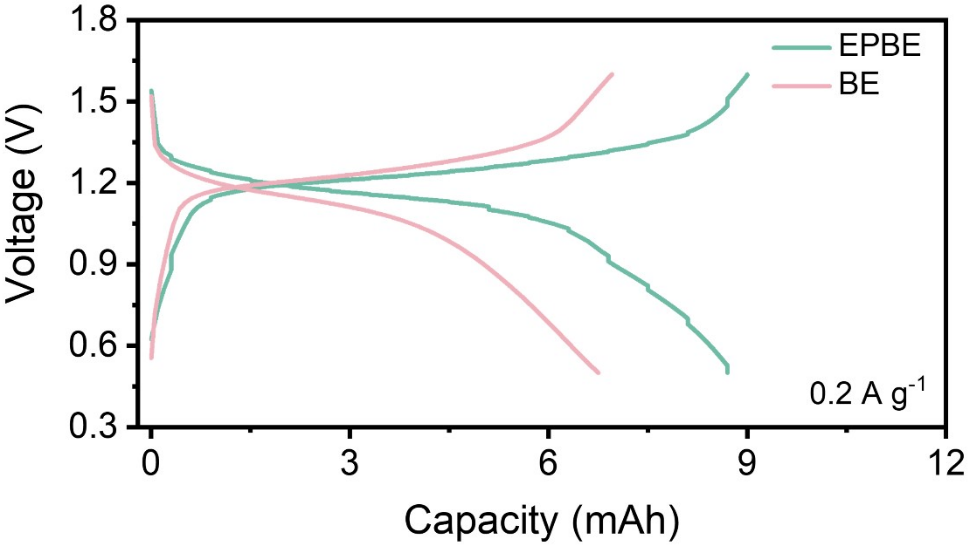

Figure S41. GCD curves of Zn||I_2 cells at 0.2 A g^{-1}

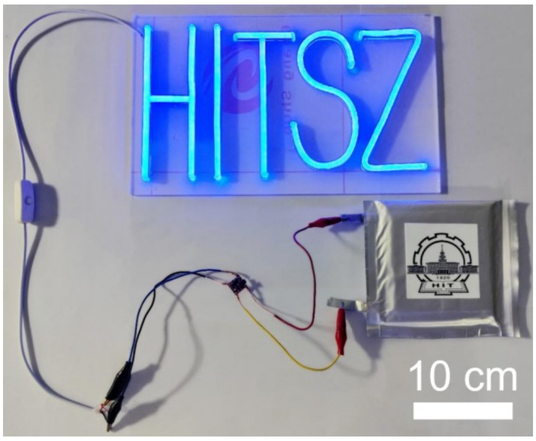

Figure S42. Demonstration of Zn||I_2 pouch cell applied for illuminating an LED light.

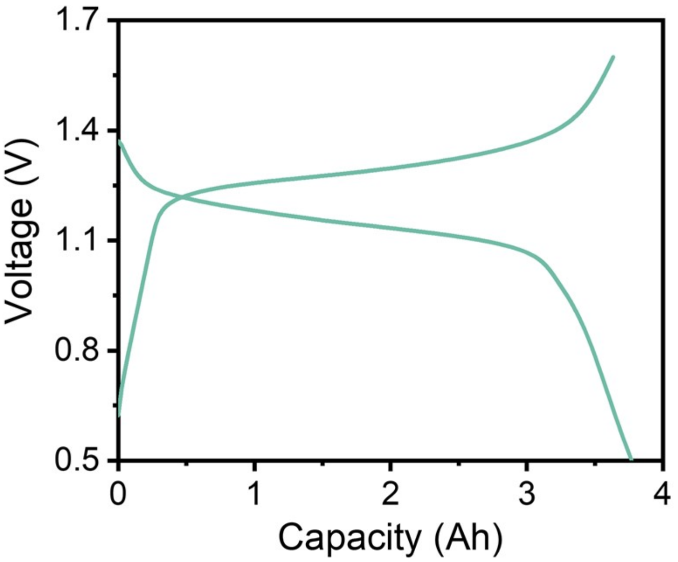

Figure S43. Charge-discharge curve of the first cycle of 3.7 Ah Zn||I_2 pouch cell.

Table S1. The comparison of electrochemical performance and specific parameters of the Zn||Zn symmetric cells reported in this work with other previous reports in Fig.3e.

Strategies	Working conditions (mA cm^{-2}-mAh cm^{-2})	Lifespan (h)	Thickness of Zn (μm)	DOD (%)	Ref.
PCA-Zn addtive	20-20	300	100	40	18
PCA-Zn electrolyte	1-1	1400	80	2.1	19
PCA-Zn addtive	20-1	1000	100	1.7	20
Tricine additive	10-10	720			40
Sc^{3+} additive	4-4	130	80	13.7	41
THF additive	1-1	2800			42
TPPS additive	1-1	2300	80	2.1	43
FEC additive	4-1	1000			44
Zn-Cu electrolyte	25-0.84	90			45
MOF additive	10-0.5	900	200	0.4	46
TBP additive	10-5	220	100	8.5	47
AQS additive	5-1	1120	100	1.7	48
EMIm$^+$ additive	20-10	600			49
SPS additive	5-5	870	100	8.5	50
TFA additive	10-1	1100			51
Sucrose additive	5-5	500	100	8.5	52
CoSA/C additive	10-2.5	1600			53
DMAC/TMP/H_2O	5-5	1650	100	8.5	54
This work	5-5	5255	100	8.5	
This work	10-10	3680	100	17	
This work	30-30	235	100	51	
This work	5-27.2	250	50	93	

References

[1] Frisch, M. J. Trucks, g. w. Schlegel, h. b. et al. Gaussian 16 Rev. A.03[CP/OL].

[2] Lu, t. Chen, f. Multiwfn: A multifunctional wavefunction analyzer. Journal of Computational Chemistry, 2012,33(5): 580-592.

[3] Zhang, j. Lu, t. Efficient evaluation of electrostatic potential with computerized optimized code. Physical Chemistry Chemical Physics, 2021,23(36): 20323-20328.

[4] Humphrey, w. Dalke, a. Schulten, k. VMD: Visual molecular dynamics. Journal of Molecular Graphics, 1996,14(1): 33-38.

[5] Kresse, G. & Furthmüller, J. Efficient iterative schemes for ab initio total-energy calculations using a plane-wave basis set. Physical review B 54, 11169 (1996).

[6] Perdew, J. P., Burke, K. & Ernzerhof, M. Generalized gradient approximation made simple. Physical Review Letters 77, 3865 (1996).

[7] Grimme, S., Antony, J., Ehrlich, S. & Krieg, H. A consistent and accurate ab initio parametrization of density functional dispersion correction (DFT-D) for the 94 elements H-Pu. J Chem Phys 132, 154104, doi:10.1063/1.3382344 (2010).

[8] Monkhorst, H. J. & Pack, J. D. Special points for Brillouin-zone integrations. Physical Review B 13, 5188-5192, doi:10.1103/PhysRevB.13.5188 (1976).